



HAL
open science

Atomic layer deposition of ZnIn_xSy buffer layers for Cu(In,Ga)Se₂ solar cells

P. Genevee, Arouna Darga, C. Longeaud, D. Lincot, F. Donsanti

► To cite this version:

P. Genevee, Arouna Darga, C. Longeaud, D. Lincot, F. Donsanti. Atomic layer deposition of ZnIn_xSy buffer layers for Cu(In,Ga)Se₂ solar cells. *Journal of Renewable and Sustainable Energy*, 2015, 7 (1), pp.013116. 10.1063/1.4906912 . hal-01253407

HAL Id: hal-01253407

<https://centralesupelec.hal.science/hal-01253407>

Submitted on 24 Aug 2020

HAL is a multi-disciplinary open access archive for the deposit and dissemination of scientific research documents, whether they are published or not. The documents may come from teaching and research institutions in France or abroad, or from public or private research centers.

L'archive ouverte pluridisciplinaire **HAL**, est destinée au dépôt et à la diffusion de documents scientifiques de niveau recherche, publiés ou non, émanant des établissements d'enseignement et de recherche français ou étrangers, des laboratoires publics ou privés.

Atomic layer deposition of ZnIn_xS_y buffer layers for $\text{Cu}(\text{In,Ga})\text{Se}_2$ solar cells

Cite as: J. Renewable Sustainable Energy 7, 013116 (2015); <https://doi.org/10.1063/1.4906912>
Submitted: 19 September 2014 . Accepted: 17 January 2015 . Published Online: 30 January 2015

P. Genevée, A. Darga, C. Longeaud, D. Lincot, and F. Donsanti



View Online



Export Citation



CrossMark

ARTICLES YOU MAY BE INTERESTED IN

[Zn\(O, S\) buffer layers by atomic layer deposition in \$\text{Cu}\(\text{In, Ga}\)\text{Se}_2\$ based thin film solar cells: Band alignment and sulfur gradient](#)

Journal of Applied Physics **100**, 044506 (2006); <https://doi.org/10.1063/1.2222067>

[Detailed Balance Limit of Efficiency of p-n Junction Solar Cells](#)

Journal of Applied Physics **32**, 510 (1961); <https://doi.org/10.1063/1.1736034>

[New insights on the chemistry of plasma-enhanced atomic layer deposition of indium oxysulfide thin films and their use as buffer layers in \$\text{Cu}\(\text{In,Ga}\)\text{Se}_2\$ thin film solar cell](#)

Journal of Vacuum Science & Technology A **36**, 061510 (2018); <https://doi.org/10.1116/1.5048124>

NEW!

Sign up for topic alerts
New articles delivered to your inbox

AIP
Publishing



Atomic layer deposition of ZnIn_xS_y buffer layers for $\text{Cu}(\text{In,Ga})\text{Se}_2$ solar cells

P. Genevée,^{1,a)} A. Darga,² C. Longeaud,² D. Lincot,¹ and F. Donsanti^{1,a)}

¹*Institut de Recherche et Développement sur l'Energie Photovoltaïque (IRDEP), UMR 7174 EDF–CNRS–Chimie ParisTech, 6 Quai Watier, 78401 Chatou, France*

²*LGEP, CNRS UMR8507, SUPELEC, Univ Paris-Sud, Sorbonne Universités - UPMC, Univ Paris 06, 11 rue Joliot-Curie, Plateau de Moulon, 91192 Gif-sur-Yvette Cedex, France*

(Received 19 September 2014; accepted 17 January 2015; published online 30 January 2015)

We report in this paper the use of ZnIn_xS_y films deposited by atomic layer deposition as cadmium free buffer layer in $\text{Cu}(\text{In,Ga})\text{Se}_2$ (CIGS) solar cells. Buffer layers with different $\text{In}/(\text{In} + \text{Zn})$ ratios over the whole composition range were prepared on glass substrate and characterized optically by transmission and reflection measurement and electrically by steady state photoconductivity and modulated photocurrent. CIGS solar cells were prepared with the different buffer layers and characterized. A compromise between the properties of In_2S_3 and ZnS was found for intermediate compositions as aimed for this study. Best efficiencies were obtained for intermediate composition ($\text{In}/(\text{In} + \text{Zn})$ close to 28 at. %) which also allows a higher open circuit voltage. Solar cell simulations allowed to point out the major role played by interface defect states in these devices. © 2015 AIP Publishing LLC. [<http://dx.doi.org/10.1063/1.4906912>]

I. INTRODUCTION

In copper indium gallium diselenide ($\text{Cu}(\text{In,Ga})\text{Se}_2$ noted CIGS), solar cells with a structure consisting of aluminum doped zinc oxide ($\text{ZnO}:\text{Al}$)/intrinsic zinc oxide (i-ZnO)/buffer layer/CIGS/molybdenum/glass, the electron transport through the conduction band depends on the conduction band offset (CBO) at the interface between the buffer layer and the absorber layer (defined as the difference between the conduction band minimum of the buffer layer and the one of the absorber layers). Optimal performance should be obtained for a conduction band offset from 0 to $+0.4\text{ eV}$ ¹ which is the case at the cadmium sulfide (CdS)/ CuInSe_2 interface.² CdS films present an n-type doping and allow an excellent passivation of the absorber thanks to a good lattice matching (2% of mismatch for $\text{CuIn}_{0.7}\text{Ga}_{0.3}\text{Se}_2$). The main drawback of CdS is its optical bandgap of about 2.4 eV which causes photocurrent losses as holes photo-generated in the buffer layer are not collected. In spite of this weakness, CdS is still the buffer layer offering the highest efficiencies (20.8%).³

From all binary compounds, none present better properties than CdS for application as buffer layer in CIGS solar cells. Thus to find buffer layers better than CdS , mixed materials with tunable electronic properties have been investigated and allowed very high efficiencies. For example, an efficiency of 18.5% was reported for the addition of oxygen to ZnS giving $\text{Zn}(\text{O,S})$ ^{4,5} and an efficiency of 18.1% was reported for the addition of magnesium to ZnO giving Zn,MgO .⁶

We have reported previously the growth of ZnIn_xS_y (ZIS) films by Atomic Layer Deposition (ALD) with a good control of film thickness and composition.⁷ The optical bandgap of the film varies with the composition from an indirect transition of 2.1 eV for pure In_2S_3 to a direct transition of 3.6 eV for pure ZnS . We expect the CBO at the interface with

^{a)}Authors to whom correspondence should be addressed. Electronic addresses: pascal-genevee@chimie-paristech.fr and frederique.donsanti@edf.fr.

$\text{CuIn}_{0.7}\text{Ga}_{0.3}\text{Se}_2$ to follow the same trend and to vary from -0.4 eV for pure In_2S_3 ⁸ to $+1.2\text{ eV}$ for pure ZnS .⁹ Moreover, ZnS based buffer layers and In_2S_3 buffer layers allow good efficiencies^{4,5,10,11} and may form a suitable surface passivation of the CIGS layer.

The aim of this study is to use ZIS buffer layers in CIGS solar cells and to observe its influence on the optoelectronic properties of the device. The influence of buffer layer composition and deposition temperature will be studied. As the buffer layer/window layer interface has been reported to impact the cell properties, the influence of the *i*-ZnO layer has also been investigated.^{12,13}

II. EXPERIMENTAL CONDITIONS

ZIS layers were synthesized by ALD on an ASM Microchemistry F-120 reactor with a $5\text{ cm} \times 5\text{ cm}$ reaction chamber. Sources used were diethylzinc ($\text{Zn}(\text{C}_2\text{H}_5)_2$ noted DEZ) and trimethylaluminum ($\text{Al}(\text{CH}_3)_3$ noted TMA) Optograde from Rohm and Haas, indium acetylacetonate ($\text{In}(\text{CH}_3\text{COCHCOCH}_3)_3$ noted $\text{In}(\text{acac})_3$) (98%) from ALFA AESAR GMBH & CO KG, H_2S (99.5%) from Messer and deionized Millipore water. Nitrogen (N_2) (99.9999%) from Messer was used as carrier and purge gas. $\text{In}(\text{acac})_3$ was heated at $(125 \pm 5)^\circ\text{C}$ while other sources were kept at room temperature.

Substrate temperatures for ZIS depositions were $(180 \pm 5)^\circ\text{C}$, $(200 \pm 5)^\circ\text{C}$, or $(220 \pm 5)^\circ\text{C}$. The growth consisted in the repetition of the following pulse and purge sequence (with their respective durations):

$$A \times \text{DEZ pulse}/\text{N}_2 \text{ purge}/\text{H}_2\text{S pulse}/\text{N}_2 \text{ purge} = 1/3/1/2 \text{ s},$$

$$B \times \text{In}(\text{acac})_3 \text{ pulse}/\text{N}_2 \text{ purge}/\text{H}_2\text{S pulse}/\text{N}_2 \text{ purge} = 1/3/1/2 \text{ s},$$

where $A = 1$ except for films of pure In_2S_3 . For this study, six couples of parameters (A , B) were chosen and are given in Table I. The corresponding compositions for films grown at 200°C were determined previously by energy-dispersive X-ray spectroscopy (EDX) on thick samples. The indium content in these films is low compared to the content expected from the rule of mixtures as discussed in a previous paper.¹⁴ Thus, the growth of mixed films requires to use parameters B larger than A . In this paper, we will name buffer layers with the ratio $\text{In}/(\text{In} + \text{Zn})$ in the thick film. For example, the couple $(A:B) = (1:50)$ leads to a ZIS layer with a ratio $\text{In}/(\text{In} + \text{Zn}) = 34\%$ which is named “ZIS 34%.” Both In_2S_3 and ZnS depositions exhibit a slightly decreasing growth rate with increasing temperature around 200°C . We expect no composition change and a negligible thickness change in the layers within the temperature range of 180°C – 220°C .

The $\text{Cu}(\text{In,Ga})\text{Se}_2$ layers used were coevaporated at Würth Solar GmbH & Co. KG and at IRDEP. These absorber layers are of industrial quality with conversion efficiencies in the range of 12%–13%. Buffer layer depositions were done directly after a potassium cyanide (KCN) etching of the absorber surface. Once buffer layers are deposited, samples are kept under vacuum.

Buffer layers were coated with an ALD *i*-ZnO layer, a sputtered *i*-ZnO layer, or no *i*-ZnO layer. The sputtered *i*-ZnO layers with a thickness of 80 nm were deposited by Radio Frequency Magnetron Sputtering (RF Sputtering) and present a high resistivity ($>10^3 \Omega\cdot\text{cm}$).

TABLE I. Composition of the different layers determined on thick samples.

A	B	Sequences in thick layers	Sequences in buffer layers	In (at. %)	Zn (at. %)	S (at. %)	In/(In + Zn) (at. %)
1	0	745	70	0	58.7	41.3	0
1	11	186	28	6.1	49.2	44.7	11
1	28	116	18	14.5	36.9	48.6	28
1	50	80	11	17.1	33.4	49.5	34
1	120	40	5	33.0	12.4	54.7	73
0	1	5000	948	41.8	0	58.2	100

The ALD i-ZnO layers were deposited in a Picosun SUNALE R-200 ALD reactor using the growth cycle DEZ pulse/N₂ purge/H₂O pulse/N₂ purge = 0.1/2/0.2/3 s at (160 ± 5) °C. The films were deposited performing a total of 250 growth cycles giving a thickness of about 50 nm and were unloaded without cooling. The resistivity of this material is close to 1 Ω·cm.

To complete the cells, 500 nm of ZnO:Al were deposited by ALD at (160 ± 5) °C in the SUNALE R-200 reactor. As presented in a previous paper, long purges (>4 s) during the growth of ZnO:Al films improve the material conductivity.¹⁵ Thus, the growth consisted in repeating the following sequence 150 times:

$$19 \times \text{DEZ pulse/N}_2\text{purge/H}_2\text{O pulse/N}_2\text{purge} = 0.1/6/0.1/4 \text{ s,}$$

$$1 \times \text{TMA pulse/N}_2\text{purge/H}_2\text{O pulse/N}_2\text{purge} = 0.1/4/0.1/6 \text{ s,}$$

giving a sheet resistance in the range of 50–60 Ω/□.

For each absorber batch, reference cells with a CdS buffer layer (30–40 nm) deposited by chemical bath deposition (CBD) and i-ZnO (80 nm)/ZnO:Al (400 nm) deposited by RF sputtering were synthesized.

Samples were mechanically scribed to delimit twelve square cells with a surface of 0.1 cm². Cells were air annealed for 10 min at 200 °C and light soaked during 30 min under AM1.5 to stabilize their response. J-V measurements were done in the dark and under AM1.5 illumination. External quantum efficiencies of some solar cells were recorded.

Buffer layer thicknesses were estimated from the thickness of thick samples using the assumption that in an ALD process, film thickness is proportional to the number of growth cycles. However, during the first cycles, the growth rate is lower due to a nucleation period. This nucleation period was estimated using a quartz crystal microbalance (QCM) as shown in a previous paper for the growth of zinc oxide.¹⁶ We found that the growth rate is constant after 70 growth cycles for ZnS while 300 cycles are needed for In₂S₃.

Optical characterizations were conducted using a PerkinElmer lambda 900 Spectrophotometer with a PELA-1000 integrating sphere. Absorption coefficients of films were determined from the transmittance (T) and the reflectance (R) spectra using the formula $\alpha = -1/t \times \ln(T/(1-R))$, where t is the film thickness.

For transport measurements (Steady-State PhotoConductivity, SSPC, Modulated PhotoCurrent, MPC), we have used several samples, with different composition (shown in Table I) and a thickness of about 100 nm, built in coplanar configuration, consisting of ZIS films deposited on a glass substrate. Subsequently, two silver paste strips were deposited to form ohmic contacts 1 cm long and 1 mm apart. SSPC were measured every 10 K between 110 and 350 K on samples fitted onto the cold finger of a dynamically pumped cryostat. Depending of the band gap value, light emitting diode (LED) with the corresponding wavelength serves for illuminating the sample. The photoconductivity was measured with the sample being illuminated by a constant flux ($F_{dc} = 10^{14}$ or 5×10^{14} or 10^{15} or 10^{16} cm⁻²·s⁻¹). The same light was used to perform MPC experiments to determine the Density Of States (DOS). MPC data were measured every 20 K between 110 and 350 K. The amplitude of the modulated flux was 4 times lower than the average flux F_{dc} and the modulation frequencies were in the range from 12 Hz to 40 kHz. Each measurement was the average of 20 acquisitions of the phase shift and modulus of the alternating current and resulted in an error of the order of 10%.

Solar cells simulations were done using SCAPS v3.2.¹⁷ The basic simulation parameters used are summed up in Table II. CIGS, ordered vacancy compound (OVC), i-ZnO, and ZnO:Al parameters are casually used parameters for simulation. Buffer parameters were chosen to be consistent with experimental results.

III. RESULTS AND DISCUSSION

A. Optical properties of ZIS films deposited on glass substrates

The optical properties of the films deposited on a glass substrate are shown in Figure 1. Figure 1(a) presents the absorption coefficient of the different films and the absorption

TABLE II. Basic parameters used in solar cells simulations with SCAPS.

Layer	CIGS	OVC	Buffer	i-ZnO	ZnO:Al
Thickness (μm)	2	0.015	0.015	0.05	0.3
Bandgap (eV)	1.15	1.35	3	3.3	3.3
Electron affinity (eV)	4.5	4.5	4.5	4.55	4.55
Dielectric permittivity (relative)	10	10	10	10	10
CB effective density of states (cm^{-3})	6.7×10^{17}	6.7×10^{17}	2×10^{19}	5×10^{18}	5×10^{18}
VB effective density of states (cm^{-3})	1.5×10^{19}	1.5×10^{19}	2×10^{19}	5×10^{18}	5×10^{18}
Electron thermal velocity ($\text{cm}\cdot\text{s}^{-1}$)	1×10^7	1×10^7	1×10^7	1×10^7	1×10^7
Hole thermal velocity ($\text{cm}\cdot\text{s}^{-1}$)	1×10^7	1×10^7	1×10^7	1×10^7	1×10^7
Electron mobility ($\text{cm}^2\cdot\text{V}^{-1}\cdot\text{s}^{-1}$)	50	50	50	50	50
Hole mobility ($\text{cm}^2\cdot\text{V}^{-1}\cdot\text{s}^{-1}$)	20	20	20	20	20
Shallow uniform donor density ND (cm^{-3})	0	1×10^{13}	5×10^{14}	1×10^{16}	1×10^{18}
Shallow uniform acceptor density NA (cm^{-3})	5×10^{15}	0	0	0	0
Absorption constant A ($\text{cm}^{-1}\cdot\text{eV}^{-0.5}$)	1×10^5	1×10^5	1×10^5	1×10^5	1×10^5

coefficient of a CdS film deposited by CBD on a glass substrate. In this figure, it can be seen that ZIS films with an indium content lower than 73 at. % are more transparent than the CdS film. The absorption coefficient of the layer ZIS 28% exhibits a straight edge consistent with a material with a high defect concentration. This was expected as ZnS and In_2S_3 have different crystal structures so that a mixture should exhibit a high concentration of defects.

Figures 1(b) and 1(c) present the curves $\alpha^{0.5} = f(E)$ and $\alpha^2 = f(E)$ exhibiting, respectively, indirect and direct optical transitions in the films.¹⁸ We can identify an indirect optical transition in indium rich samples which varies from 2.0 eV for pure In_2S_3 to 2.7 eV for ZIS 11%. The bandgap widening can be attributed to the addition of zinc in indium sulfide forming a compound optically close to ZnIn_2S_4 with a bandgap reported between 2.5 eV (Ref. 19) and 2.86 eV.²⁰ Two

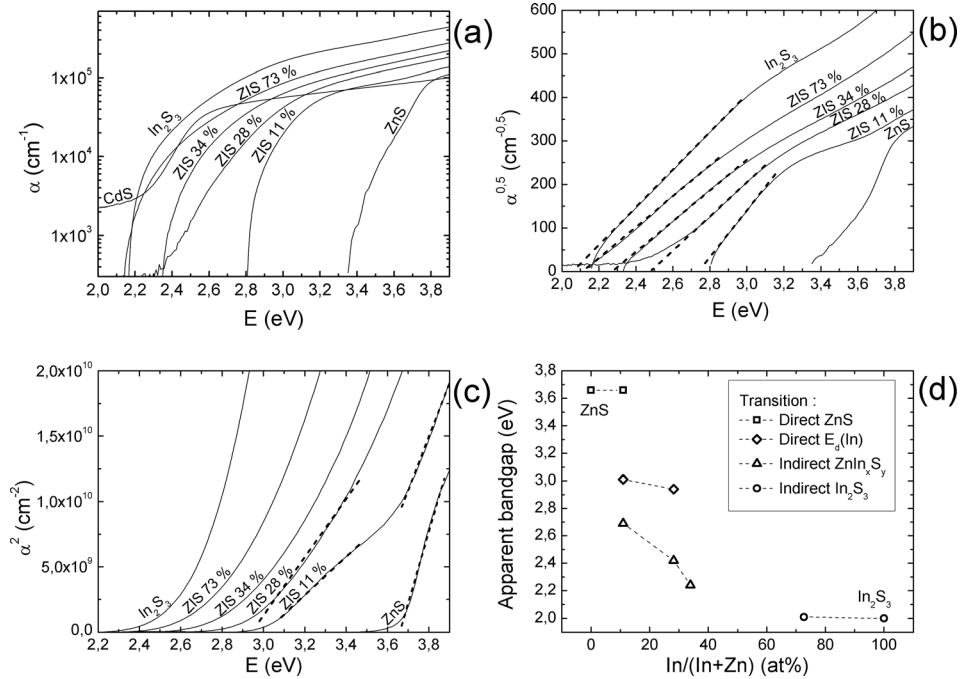


FIG. 1. Evolution of optical properties with the In/(In + Zn) ratio. (a) $\alpha = f(E)$, (b) $\alpha^{0.5} = f(E)$, (c) $\alpha^2 = f(E)$, and (d) apparent bandgap.

direct transitions are found in zinc rich samples. The first one at 3.65 eV corresponds to the fundamental band to band transition in ZnS. The second one at 3.0 eV can be attributed to optical transitions between the valence band of ZnS and the donor level of indium impurities in substitution of zinc atoms. The indium donor level in ZnS has been reported to lie at about 0.5 eV beneath the conduction band which is in good agreement with our measurements.²¹

Finally, the optical transition energies identified are summed up in Figure 1(d) as a function to the ratio In/(In + Zn).

B. Electrical properties of ZIS films deposited on glass substrates

As shown by optical measurements, the addition of zinc in indium sulfide can lead to a formation of defect state within the ZIS films band gap. These defects can also affect electronic transport properties of ZIS buffer layers, and thus the resulting solar cells electrical properties. Depending on the disorder level introduced by the addition of zinc in indium sulfide, these defects can be a simple level like the donor level of indium impurities in substitution of zinc atoms or band of defects. We have used SSPC technique to determine ZIS electronic transport properties and MPC to probe defect state density within the ZIS films band gap.

1. Dark conductivity

Figure 2 shows the temperature dependence of the dark conductivity (σ_d) for ZIS samples with different values of In/(In + Zn) ratio.

In the temperature range $300\text{ K} < T < 450\text{ K}$, the data follow a temperature dependence of the form

$$\sigma_d = \sigma_0 \exp\left[-\frac{E_a}{k_B T}\right], \quad (1)$$

where E_a is the activation energy and σ_0 a pre-exponential factor. Values of E_a and σ_d at 300 K are reported in Table III.

σ_d at 300 K is observed to increase with In/(In + Zn) ratio, while the activation energy decreases with In/(In + Zn) ratio. Assuming that the activation energy gives the position of the Fermi level at 0 K with respect to the conduction band edge and considering the values of the optical band gap, we can give the image of the evolution of the band edges with respect to the Fermi level in our ZnIn_xS_y alloys shown in Figure 3.

Though the activation energy decreases with In/(In + Zn) ratio, one can note that the alloys get more doped. To gain a better insight on the evolution of the edge of the conduction band

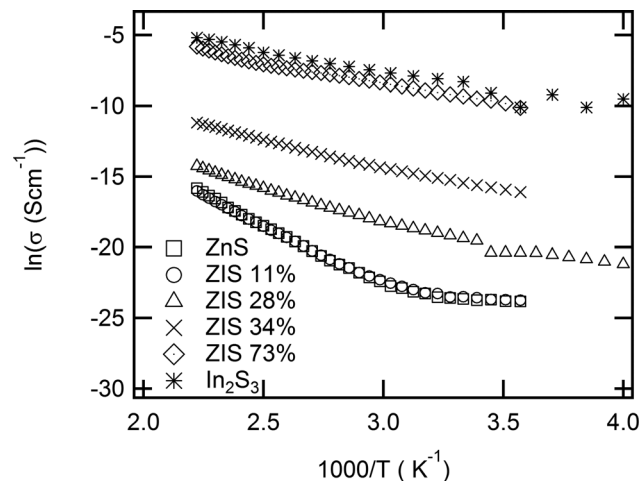


FIG. 2. Evolution of the layers conductivity as a function of the temperature.

TABLE III. Activation energy and conductivity at 300 K determined from the measurements.

Samples	Thickness (nm)	Ea (eV)	σd @ 300K ($\Omega^{-1}\cdot\text{cm}^{-1}$)	Characteristic energy from MPC Eu (meV)
ZnS	95	0.75	4.77×10^{-11}	...
ZIS 11%	135	0.74	6.07×10^{-11}	...
ZIS 28%	120	0.42	2.10×10^{-9}	43
ZIS 34%	137	0.34	1.10×10^{-7}	34
ZIS 73%	183	0.25	8.80×10^{-5}	17
In ₂ S ₃	100	0.2	2.45×10^{-4}	17

with increasing the In/(In + Zn) ratio, we have investigated the trap state density within the band gap for different ZIS alloys via MPC.

2. Defects spectroscopy

In MPC experiments, the sample is illuminated by a monochromatic light flux modulated with angular frequency ω , while the induced alternating photo current is measured in a coplanar geometry. From the modulus of the alternating photocurrent and its phase shift ϕ with respect to the excitation light, one can deduce the quantity $N(E\omega) \cdot C_n \cdot \mu_n^{-1}$ that we shall call the MPC-DOS according to the following equations:^{22,23}

$$\frac{N(E\omega)C_n}{\mu_n} = \frac{2}{\pi k_B T} q G_{ac} \frac{\sin(\phi)}{|\sigma_{ac}|}, \quad (2)$$

with

$$E_c - E_\omega = k_B T \ln \left(\frac{C_n N_c}{\omega} \right), \quad (3)$$

where $N(E_\omega)$ is the density of states at an energy E_ω , C_n is the capture coefficient of the states trapping the free carriers (electrons in ZIS), and $|\sigma_{ac}|$ is the modulus of the alternating photoconductivity resulting from the modulated generation rate G_{ac} . Figure 4 shows an example of spectra calculated by applying Eqs. (2) and (3) to the MPC data obtained at various temperatures and angular frequencies for ZIS films with 28% of In/(In + Zn) ratio.

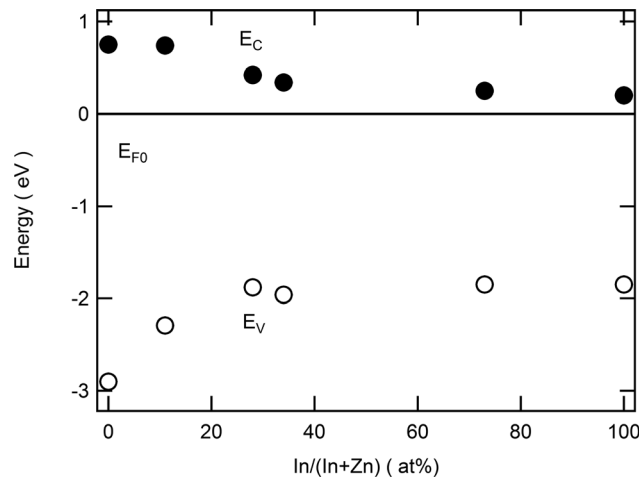


FIG. 3. Evolution of the band edges with respect to the Fermi level.

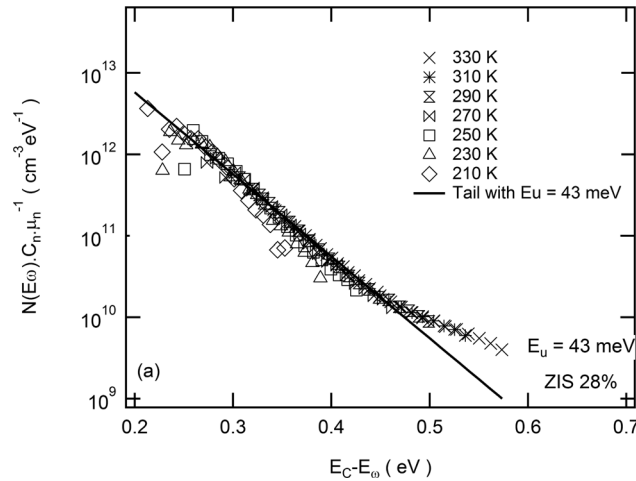


FIG. 4. Example of MPC density of states spectra for sample with ZIS of 28%.

By using a LED light source of wavelength $\lambda = 385$ nm, the photocurrent generated by ZIS samples with low values of the $\text{In}/(\text{In} + \text{Zn})$ ratio (large band gap) is not enough for performing MPC measurements. As is shown in Figure 4, and for most of the studied samples, it can be seen that the parts of the spectra obtained at high frequency, i.e., the parts closest to the conduction band edge, are all converging in a single, well defined envelope describing an exponentially decreasing conduction band tail (CBT). The characteristic energy (E_u) of the exponentially decaying conduction band tail decreases with increasing the $\text{In}/(\text{In} + \text{Zn})$ ratio, indicating the decrease of the disorder. Values of E_u are reported in Table III.

The highest value of E_u is obtained with the ZIS 28% sample in accordance with optical measurements (see Table III). The higher disorder in the buffer layer may involve more defect states and thus recombination in this layer or at its interfaces in the solar cells.

C. Solar cells properties

1. Effect of the buffer layer composition

All buffer layers were used in solar cells and tested with a sputtered i-ZnO layer and an ALD ZnO:Al layer. Buffer layers thicknesses were about 15 nm except for pure ZnS which was only 5 nm thick because a thicker layer would block the photocurrent through the solar cell as it has a very low conductivity (see Table III).^{9,24}

Figure 5 shows the J-V curves of solar cells with six ZIS layers of different compositions. A seventh curve shows the J-V of the reference cell with a CdS buffer layer. Table IV sums up the corresponding solar cells parameters.

We note that the In_2S_3 buffer layer gives a J-V characteristic close to the one of the CdS buffer layer. Its short circuit current density (J_{sc}) is close to that with CdS but its open circuit voltage is lower by 20 mV. The fill factor (FF) is also weaker than with CdS. As shown in Table III, In_2S_3 buffer layer is relatively doped with a small characteristic energy, thus, a negative band offset together with defect states at the CIGS/buffer interface may be responsible for an increase of interface recombination, and therefore a lower V_{oc} and FF as it was shown by Minemoto *et al.*¹ This result is in good agreement with the negative band offset measured by Sterner *et al.* at the CIGS/ In_2S_3 interface.⁸

We note that the lowering of the $\text{In}/(\text{In} + \text{Zn})$ ratio down to 34% does not strongly change the cell response. It mainly decreases the FF and slightly improves the J_{sc} but the V_{oc} is unchanged.

The ZIS 28% buffer layer leads to a different solar cell behavior. The corresponding solar cell has a J_{sc} equivalent to those of indium rich buffers and presents an improved V_{oc} up to

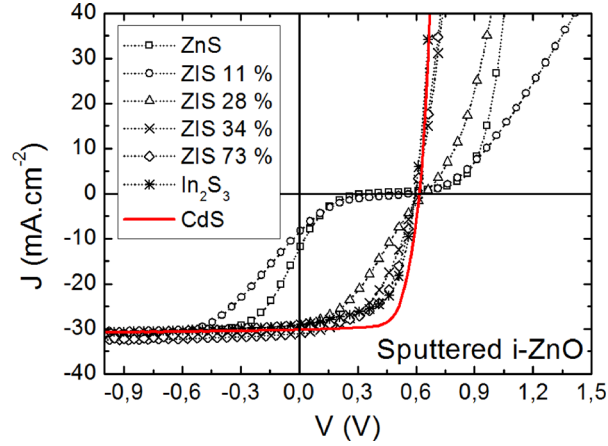


FIG. 5. Current density versus voltage (J-V) characteristics of solar cells as a function of the buffer layer composition with a sputtered i-ZnO layer. Illumination AM1.5 $100 \text{ mW}\cdot\text{cm}^{-2}$.

0.64 V, which is 30 mV higher than that of the reference cell. The efficiency is limited by a weak FF.

The J-V curve corresponding to the ZnS buffer layer exhibits an S shape which is typical for a solar cell with a high recombination rate of photo-generated electrons at the interface buffer/CIGS.

The same behavior is observed with the ZIS 11% for which the J_{sc} is a bit lower. However, the difference between the two J_{sc} is low if we consider that the ZIS 11% layer is three times thicker than the ZnS one.

Figure 1(c) evidenced indium impurities in substitution of zinc atoms in ZnS. Given the quantity of indium in the material, we can explain the improvement of the solar cell by the formation of an impurity-induced band in the gap of ZnS allowing a satisfactory electron transport with a reduced barrier height by 0.5 eV.

To explain the evolution observed between pure In_2S_3 and ZIS 28%, series of solar cell simulations were done using SCAPS. Different parameters allowed to explain the increase of V_{oc} together with the reduction of the fill factor. As we physically only change the buffer layer, we focus on the buffer layer properties and its interfaces. We consider:

- A negative CBO at the CIGS/buffer interface.
- A positive CBO at the CIGS/buffer interface.
- Acceptor defects at the CIGS/buffer interface.
- Acceptor defects at the i-ZnO/buffer interface.

Figure 6 shows the simulated J-V responses under illumination and the evolution of V_{oc} .

The first hypothesis to explain the experimental evolution is the formation of a cliff (negative CBO) at the interface CIGS/buffer. Mixed ZIS layers are very complex and may be composed of several phases as shown in the optical study. We can deduce from the study of Vigil *et al.*²⁵ that

TABLE IV. Parameters of solar cells as a function of the buffer layer for a sputtered i-ZnO layer.

In/(In + Zn) (at. %)	V_{oc} (mV)	J_{sc} ($\text{mA}\cdot\text{cm}^{-2}$)	FF (%)	Efficiency (%)
0	380	12.4	11.4	0.5
11	587	8.6	9.6	0.5
28	646	29.4	34.6	6.6
34	595	31.0	47.7	8.8
73	597	29.8	56.2	10.0
100	595	29.1	60.1	10.4
Reference CdS	615	30.3	70.7	13.1

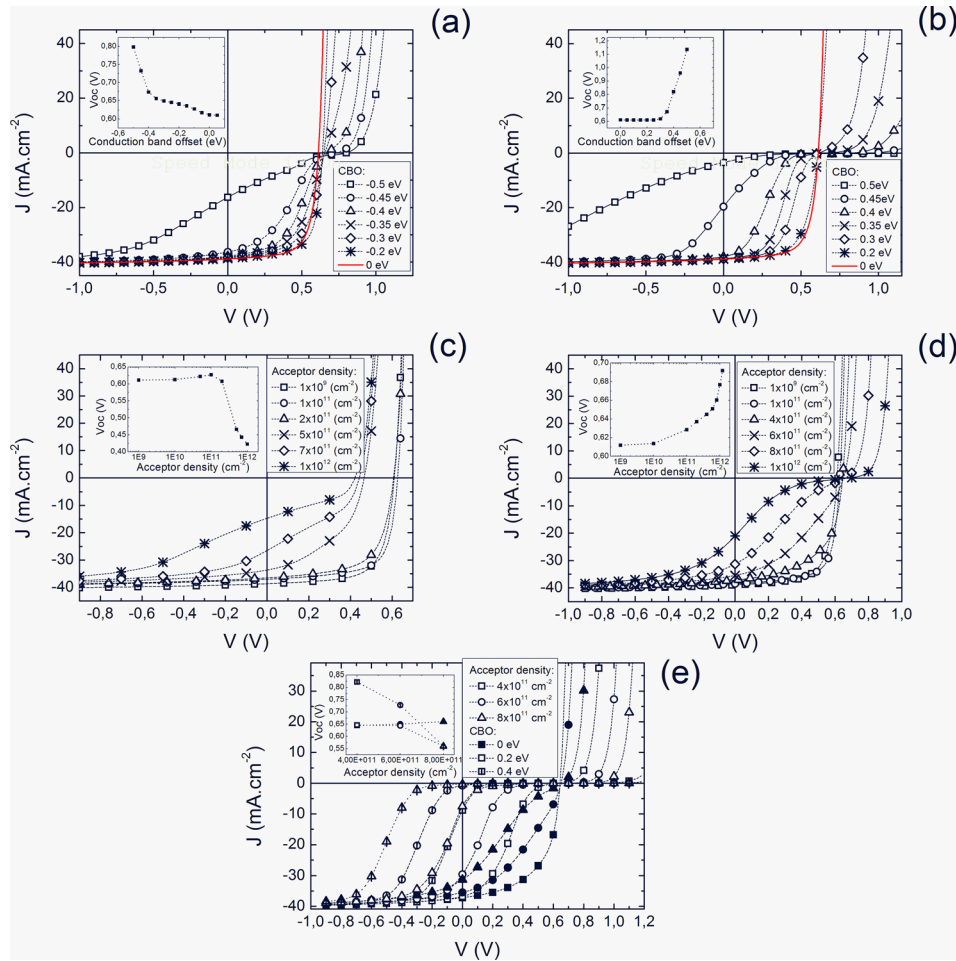


FIG. 6. Simulated J-V characteristics. Insets show the evolution of V_{oc} . (a) J-V characteristics of solar cells simulated with different negative conduction band offsets. (b) J-V characteristics of solar cells simulated with different positive conduction band offsets. (c) J-V characteristics of solar cells simulated with different densities of acceptor at the CIGS/buffer interface (without conduction band offset). (d) J-V characteristics of solar cells simulated with different densities of acceptor at the i-ZnO/buffer interface (without conduction band offset). (e) J-V characteristics of solar cells simulated with different densities of acceptor at the i-ZnO/buffer interface with positive conduction band offsets.

$ZnIn_2S_4$ exhibits an electron affinity close to 5.0 eV which is higher than that of In_2S_3 (about 4.65 eV). This indicates that such mixed materials can lead to the formation of either a spike (ZnS crystallites) or a cliff ($ZnIn_2S_4$ crystallites). Another particularity of the mixed layers is that they are amorphous like and present the advantage to lower the stress at the interface with CIGS and thus the density of defect states due to dislocations at the interfaces. If we assume a low defect state density and the formation of $ZnIn_2S_4$ crystallites, the formation of a cliff can explain the increase of V_{oc} and decrease of FF as observed in Figure 6(a).

The second hypothesis is the formation of a spike (positive CBO) at the CIGS/buffer interface which also leads to an increased V_{oc} as seen in Figure 6(b). We note that compared to the cliff, the spike leads to sharper S like J-V characteristics with a larger extent in the positive voltage due to the electron barrier effect.

The third hypothesis is an increase of acceptor defects at the CIGS/buffer interface. In this case, the V_{oc} slightly increases with the density and then decreases as seen in Figure 6(c). An S shape appears only once the V_{oc} starts to get lower. This hypothesis is not compatible with the experimental observation.

The fourth hypothesis is an increase of acceptor defects at the i-ZnO/buffer interface. We observe, in Figure 6(d), that the increase of this parameter can increase the V_{oc} and decrease

the fill factor at the same time. In this case, the extent of the J-V in the positive voltage is low but slightly higher than in the case of cliffs.

From the different trends observed, the curve ZIS 28% in Figure 5 may be best reproduced with a 0.35 eV cliff or with $6 \times 10^{11} \text{ cm}^{-2}$ acceptor defects at the i-ZnO/buffer interface. In both cases, the Voc increase is about 40 mV which is consistent with the experimental increase observed.

The second explanation (acceptors) is consistent with the MPC measurements as the disorder in ZIS layers is found to rise when the indium content is decreased down to ZIS 28%. Physically, these acceptors states generate some negative charges which modify the electric field in the solar cell. When the density is increased, the electric field decreases in the absorber layer and increases in the ZnO layer. It slightly degrades the carrier collection in the absorber but reduces interface losses. It can be seen as a possibility to tune the electric field in the solar cell.

Figure 6(e) shows the results of simulation when acceptors at the i-ZnO/buffer interface are considered together with a spike. In the case of high acceptor density ($>4 \times 10^{11} \text{ cm}^{-2}$), a spike may not involve any Voc increase which would explain why ZnS and ZIS 11% buffers do not lead to such increase.

Finally, External quantum efficiencies of the solar cells were recorded. In Figure 7, we clearly see the impact of the buffer layer optical properties on the cell response.

In the case of the reference solar cell, we note a good response in the long wavelengths down to 540 nm. For wavelengths below 540 nm we observe high losses due to light absorption in the CdS layer.

In the case of the In_2S_3 buffer layer, we observe a lower response in the long wavelength and losses due to light absorption in the buffer layer for wavelength below 600 nm. However, the In_2S_3 is about three times thinner than the CdS layer and cause a lower light absorption. This explains the better response than that of the reference cell for wavelength below 520 nm.

In the case of the ZnS buffer layer, we note a response below 0.6 for all wavelength which indicates interface recombination of the photocurrent. We also note that no supplementary losses are observed in the short wavelength which is consistent with the very wide bandgap of ZnS (ca. 3.6 eV).

The buffer layers of intermediate composition give interesting responses. Buffers ZIS 11%, ZIS 28%, and ZIS 34% allow a response equivalent to the one of In_2S_3 for wavelength above 600 nm and an improved response below 600 nm thanks to a lower absorption of light. These buffer layers may allow the best compromise between optical and electronic properties.

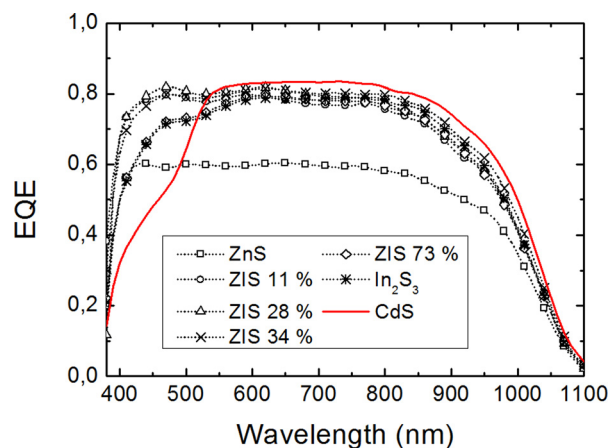


FIG. 7. External quantum efficiency of solar cells with different buffer layers and with a sputtered i-ZnO layer.

2. Effect of the *i*-ZnO layer

In Figure 8, we present the J-V characteristics of solar cells without any *i*-ZnO layer and with an ALD *i*-ZnO layer. The comparison of the J-V responses for the different *i*-ZnO layers (Figures 5 and 8) lets appear a clear trend. For buffer layers of composition close to In_2S_3 , the J-V responses are weakly dependent on the *i*-ZnO layer. However, for zinc rich buffer layers (ZnS and ZIS 11%), the *i*-ZnO layer strongly influences the J-V responses. Using ALD *i*-ZnO, the responses exhibit a narrow kink (extent over 0.7 V) while with sputtered *i*-ZnO, this kink extends over up to 1.5 V.

When the *i*-ZnO layer is changed, it also changes the *i*-ZnO/buffer interface properties. We observe in Figure 6(e) that a higher acceptor density at this interface leads to a larger extent of the kink when a spike is involved. Also, in Figure 9 we show J-V simulated with different *i*-ZnO thicknesses considering a high density of acceptor defects ($6 \times 10^{11} \text{ cm}^{-2}$) at the *i*-ZnO/buffer interface. The increase of *i*-ZnO thickness in this case involves a higher V_{oc} and a lowering of the FF. It can be assumed that a higher *i*-ZnO thickness enhances the impact of the acceptors. The behaviors corresponding to the three different *i*-ZnO layers may be explained as follows:

- Solar cells with no *i*-ZnO may exhibit lower V_{oc} which is predicted from Figure 9 due to its low *i*-ZnO thickness. The kink extent obtained with the ZnS buffer is very low as no *i*-ZnO enhances the impact of acceptors.
- Solar cells with ALD *i*-ZnO have a small *i*-ZnO thickness with a moderate resistivity. It leads to increased V_{oc} but not to large kink extents.

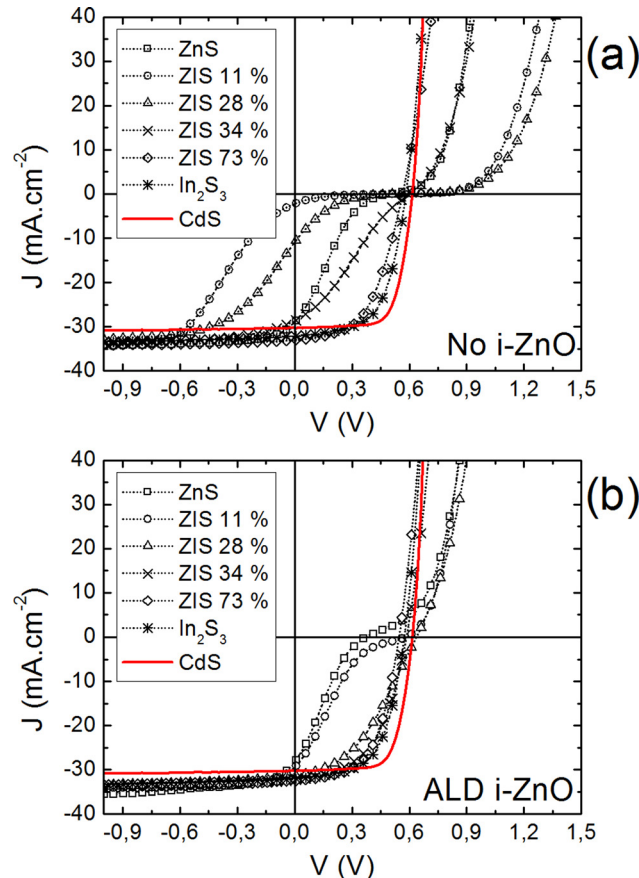


FIG. 8. J-V characteristics of solar cells with different buffer layers: (a) without any *i*-ZnO layer and (b) with an *i*-ZnO layer deposited by ALD.

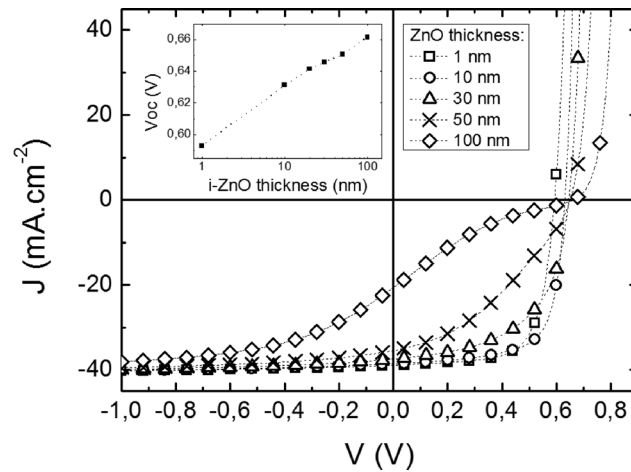


FIG. 9. Simulated J-V characteristics with $6 \times 10^{11} \text{ cm}^{-2}$ acceptor defects at the i-ZnO/buffer interface for different i-ZnO thicknesses.

- Solar cells with sputtered i-ZnO have a larger i-ZnO thickness with a high resistivity. It logically leads to high V_{oc} and large kink extents.

3. Effect of the buffer layer deposition temperature

In a second time, cells were fabricated with buffer layers of composition $\text{In}/(\text{In} + \text{Zn})$ close to 28 at. % at different temperatures. Figure 10 shows the J-V characteristics of these cells and Table V sums up the cells parameters. The solar cell performance clearly increases when the buffer layer deposition temperature decreases. This improvement is mainly due to a better fill factor and a higher open circuit voltage which is over the one of the reference cell for a deposition temperature of 180°C . We notice that an S shape is observable at a deposition temperature of 220°C while the shape is closer to a normal cell at 180°C . According to Figure 6(e), the improvement of cells properties while decreasing the deposition temperature could be attributed to a reduction of defect states at the i-ZnO/buffer interface while the CIGS/buffer interface may exhibit a narrow spike ($<0.2 \text{ eV}$). It is known that sodium impurities from the CIGS layer can diffuse through the buffer layer during its deposition. Laurencic *et al.* have shown that some defect states related to sodium diffusion are located at the i-ZnO/buffer interface.¹³ A lower deposition temperature limits the diffusion of sodium which could explain a lower level of

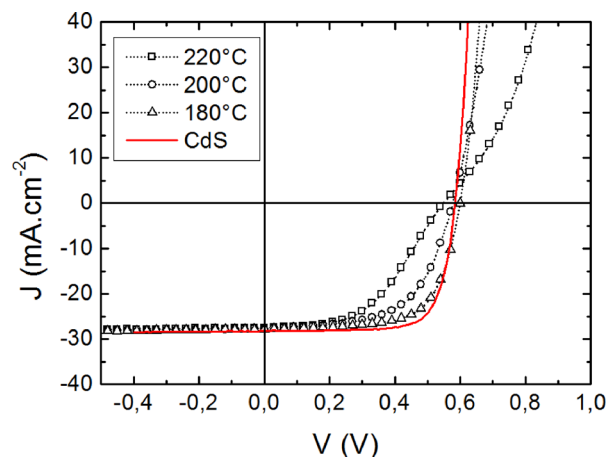


FIG. 10. J-V characteristics of solar cells with buffers of indium content $\text{In}/(\text{In} + \text{Zn})$ close to 28 at. % as a function of the buffer layer deposition temperatures. Illumination $\text{AM1.5 } 100 \text{ mW}\cdot\text{cm}^{-2}$.

TABLE V. Parameters of solar cells as a function of the buffer layer deposition temperature.

Temperature (°C)	Voc (mV)	Jsc (mA·cm ⁻²)	FF (%)	Efficiency (%)
180	600	27.8	66.9	11.2
200	577	27.6	59.0	9.4
220	553	27.6	60.0	9.2
Reference CdS	585	28.2	74.7	12.3

defect states at the i-ZnO/buffer interface and the improved Voc and FF. By changing furthermore the deposition parameters, it should be possible to improve the interfaces of the buffer layer while benefiting from its superior transparency.

IV. CONCLUSION

CIGS solar cells with ALD ZnIn_xS_y buffer layers of different compositions have been realized. Cells with indium rich buffer layers showed good J-V responses but with lower parameters than those of the CdS reference, which are attributed to the cliff together with defects at the interface CIGS/Buffer layer. Cells with zinc rich buffer layers suffer from recombination caused by a high spike at this interface which degrades its properties. Between these two extrema, an interesting compromise has been found using a ZIS 28%. This material of intermediate composition exhibits a higher transparency than CdS or In₂S₃. Moreover, it allowed to increase the cell open circuit voltage over the one of the CdS reference, which is quite unusual with alternative cadmium free buffer layers.

The modification of the i-ZnO layer highly impacted the cells responses while the lowering of the buffer layer deposition temperature, allowed to reach a conversion efficiency close to that of the reference. The most consistent hypothesis to explain the different cells responses observed is the modification of the i-ZnO thickness, the CBO at CIGS/buffer interface and the defect state density at the i-ZnO/buffer layer interface. This high contribution of defect states is consistent with the high disorder in the material pointed out by optical and MPC characterizations. This mixed ZnIn_xS_y material may be promising as new buffer layer but its thickness and deposition parameters need to be further optimized.

ACKNOWLEDGMENTS

The authors thank Würth Solar for providing coevaporated CIGS layers.

- ¹T. Minemoto, T. Matsui, H. Takakura, Y. Hamakawa, T. Negami, Y. Hashimoto, T. Uenoyama, and M. Kitagawa, *Sol. Energy Mater. Sol. Cells* **67**, 83 (2001).
- ²D. Schmid, M. Ruckh, and H. W. Schock, *Sol. Energy Mater. Sol. Cells* **41–42**, 281 (1996).
- ³P. Jackson, D. Hariskos, R. Wuerz, W. Wischmann, and M. Powalla, *Phys. Status Solidi RRL* **8**, 219 (2014).
- ⁴U. Zimmermann, M. Ruth, and M. Edoff, in *Proceedings of the 21st European Photovoltaic Solar Energy Conference* (WIP-Renewable Energies, Dresden, Germany, 2006), pp. 1831–1834.
- ⁵R. N. Bhattacharya, M. A. Contreras, and G. Teeter, *Jpn. J. Appl. Phys., Part 2* **43**, L1475 (2004).
- ⁶C. Platzer-Björkman, A. Hultqvist, J. Pettersson, and T. Törndahl, in *Proceedings of SPIE*, edited by F. H. Teherani, D. C. Look, C. W. Litton, and D. J. Rogers (San Francisco, California, USA, 2010), p. 76030F -76030F -9.
- ⁷P. Genevée, F. Donsanti, G. Renou, and D. Lincot, *J. Phys. Chem. C* **115**, 17197 (2011).
- ⁸J. Sterner, J. Malmström, and L. Stolt, *Prog. Photovoltaics: Res. Appl.* **13**, 179 (2005).
- ⁹C. Platzer-Björkman, T. Törndahl, D. Abou-Ras, J. Malmström, J. Kessler, and L. Stolt, *J. Appl. Phys., Part 1* **100**, 044506 (2006).
- ¹⁰N. Naghavi, S. Spiering, M. Powalla, B. Cavana, and D. Lincot, *Prog. Photovoltaics: Res. Appl.* **11**, 437 (2003).
- ¹¹S. Spiering, F. Kessler, and W. Wischmann, in *Proceedings of the 26th European Photovoltaic Solar Energy Conference* (WIP-Renewable Energies, Hamburg, Germany, 2011), pp. 2886–2889.
- ¹²N. Naghavi, G. Renou, V. Bockelee, F. Donsanti, P. Genevée, M. Jubault, J. F. Guillemoles, and D. Lincot, *Thin Solid Films* **519**, 7600 (2011).
- ¹³C. Laurencic, M. Buffiere, L. Arzel, and N. Barreau, in *2011 IEEE 37th Photovoltaic Specialists Conference (PVSC)* (IEEE, 2011), pp. 002746–002748.
- ¹⁴P. Genevée, F. Donsanti, N. Schneider, and D. Lincot, *J. Vac. Sci. Technol., A* **31**, 01A131 (2013).
- ¹⁵P. Genevée, F. Donsanti, G. Renou, and D. Lincot, *Appl. Surf. Sci.* **264**, 464 (2013).
- ¹⁶E. B. Yousfi, J. Fouache, and D. Lincot, *Appl. Surf. Sci.* **153**, 223 (2000).

- ¹⁷M. Burgelman, P. Nollet, and S. Degrave, "Modelling polycrystalline semiconductor solar cells," *Thin Solid Films* **361–362**, 527 (2000).
- ¹⁸J. Pankove, *Optical Processes in Semiconductors* (Dover, New York, 1975).
- ¹⁹L. Hernández, O. Vigil, and F. González, *Phys. Status Solidi* **36**, 33 (1976).
- ²⁰A. Borghesi, G. Guizzetti, and L. Nosenzo, *Prog. Cryst. Growth Charact.* **13**, 97 (1986).
- ²¹E. F. Apple and F. E. Williams, *J. Electrochem. Soc.* **106**, 224 (1959).
- ²²R. Brüggemann, C. Main, J. Berkin, and S. Reynolds, *Philos. Mag. B* **62**, 29 (1990).
- ²³C. Longeaud and J. P. Kleider, *Phys. Rev. B* **45**, 11672 (1992).
- ²⁴M. M. Islam, S. Ishizuka, A. Yamada, K. Sakurai, S. Niki, T. Sakurai, and K. Akimoto, *Sol. Energy Mater. Sol. Cells* **93**, 970 (2009).
- ²⁵O. Vigil, S. Lopez, E. Morris, O. Calzadilla, and F. Leccabue, *Sol. Energy Mater.* **16**, 315 (1987).